

Article

# Effect of Immersion in Simulated Body Fluid on the Mechanical Properties and Biocompatibility of Sintered Fe–Mn-Based Alloys

Zhigang Xu, Michael A. Hodgson and Peng Cao \*

Department of Chemical and Materials Engineering, University of Auckland, Private Bag 92019, Auckland 1142, New Zealand; zxu886@aucklanduni.ac.nz (Z.X.); ma.hodgson@auckland.ac.nz (M.A.H.)

\* Correspondence: p.cao@auckland.ac.nz; Tel.: +64-9-923-6924

Academic Editor: Ian Baker

Received: 17 August 2016; Accepted: 30 November 2016; Published: 7 December 2016

**Abstract:** Fe–Mn-based degradable biomaterials (DBMs) are promising candidates for temporary implants such as cardiovascular stents and bone fixation devices. Identifying their mechanical properties and biocompatibility is essential to determine the feasibility of Fe–Mn-based alloys as DBMs. This study presents the tensile properties of two powder metallurgical processed Fe–Mn-based alloys (Fe–28Mn and Fe–28Mn–3Si, in mass percent) as a function of immersion time in simulated body fluid (SBF). In addition, short-term cytotoxicity testing was performed to evaluate the in vitro biocompatibility of the sintered Fe–Mn-based alloys. The results reveal that an increase in immersion duration deteriorated the tensile properties of both the binary and ternary alloys. The tensile properties of the immersed alloys were severely degraded after being soaked in SBF for  $\geq 45$  days. The ion concentration in SBF released from the Fe–28Mn–3Si samples was higher than their Fe–28Mn counterparts after 7 days immersion. The preliminary cytotoxicity testing based on the immersed SBF medium after 7 days immersion suggested that both the Fe–28Mn–3Si and Fe–28Mn alloys presented a good biocompatibility in Murine fibroblast cells.

**Keywords:** Fe–Mn-based alloys; powder sintering; tensile properties; immersion; biocompatibility

## 1. Introduction

Fe-based alloys proposed for degradable biomaterials (DBMs) are commonly designed for temporary implants such as cardiovascular stents and bone fixation devices [1–3]. So far, a variety of Fe-based systems such as Fe–Mn, Fe–Pd and Fe–Mn–Si [1–6] has been or are being developed for the potential applications. The degradability of Fe-based DBMs can avoid various complications, such as chronic inflammation, thrombosis, in-stent restenosis [7,8] or even a second surgery to remove the implants [9,10], compared to the corrosion-resistant implants such as stainless steels 316L, Ti-based and Co–Cr-based alloys [11–15].

Fe-based DBMs for load-bearing applications are exposed to an aggressive and corrosive physiological environment while in the human body [16,17]. The degradation of the implants leads to a decrease in their mechanical properties and finally loss of their mechanical integrity. Consequently, this seriously affects the life span of Fe-based degradable implants. So far, the majority of the available data on mechanical performance of Fe-based DBMs has implied that the mechanical properties of fabricated Fe-based DBMs were adequate to support the healing of diseased tissues [1,18,19]. The available data, however, cannot reflect the real mechanical properties of Fe-based implants after serving in the human body for a certain period. This is because current data were from the initial mechanical properties of the as-fabricated Fe–Mn-based alloys without implanting in a physiological environment. In other words, those current mechanical tests ignored the implantation time dependence

of mechanical properties of Fe–Mn-based DBMs in a corrosive physiological environment. In this case, it is important to investigate the evolution of the mechanical properties of the biomaterials implanted in the human body as a function of implanted time, in order to better predict the life span of the designed Fe–Mn-based DBMs.

Biocompatibility is a unique feature of biomaterials over any other materials. Biomaterials that exhibit abnormal host responses in a host could cause a series of complications such as inflammation, cytotoxicity, allergy problems and detrimental immunological response [20–24]. To ensure a mutually acceptable co-existence of biomaterials and tissues in the human body, a comprehensive biocompatibility trial both *in vitro* and *in vivo* should be carried out for any synthetic biomaterials. In general, biocompatibility is determined mainly by assessment of cytotoxicity, hemocompatibility, physical irritation, mutagenesis and/or carcinogenesis, and cell function [25,26]. In this case, *in vitro* cytotoxicity testing is a compulsory step that should be carried out before the application of the proposed biomaterials.

An immersion test in a simulated body fluid (SBF) is considered an effective way to simulate and predict the implantation time dependence of mechanical properties of Fe–Mn-based DBMs in the human body. In this study, the tensile properties of the powder formed and sintered Fe–Mn-based alloys were investigated for the first time, as a function of immersion time in SBF. In addition, a short-term *in vitro* cytotoxicity of the sintered Fe–Mn-based alloys was evaluated.

## 2. Materials and Methods

### 2.1. Powder Preparation

Elemental Fe, Mn and Si powders with high purities (see details in Ref. [3]) were used as the as-received raw materials in this study. Two types of powder mixture were prepared. One is the ternary system comprised of 69% Fe, 28% Mn and 3% Si (all in mass percent); the other is the binary system consisting of 72% Fe and 28% Mn. Both the ternary and binary powder mixtures were simply mixed for 10 h in a tubular mixer (T2F, Glen Mills, Clifton, NJ, USA) and subsequently mechanically milled (MM) for 5 h in a planetary ball mill (Pulverisette 6, Fritsch, Idar-Oberstein, Germany) under Ar atmosphere to minimize the oxidation of the powders. A stainless steel (SS) jar with a volume of 225 mL and SS balls with a diameter of 6 mm were employed. The ball-to-powder ratio was 5:1. The jar was rotated at 275 rpm, and no lubrication or process control agents were employed during the MM. Details on the particle size, morphologies, purities and MM parameters of these particles are shown in the previous published work in Ref. [3].

### 2.2. Press and Sinter

The MM powder mixture was pressed under a uniaxial pressure of 400 MPa at room temperature. The green compacts were 40 mm in length, 16 mm in width and 5 mm in height. The green compacts were sintered in a vacuum furnace (VS-020203, Advanced Corporation for Materials & Equipments Co., Ltd., Changsha, China) under a vacuum degree of  $5 \times 10^{-3}$  Pa. The heating rate was 10 °C/min if the temperature was  $\leq 800$  °C and 5 °C/min if the temperature was  $> 800$  °C. All compacts were isothermally held at 1200 °C for 3 h, followed by furnace cooling.

### 2.3. Immersion Testing

Immersion testing of all the sintered samples was conducted in SBF which has similar ion concentrations to human blood plasma, where  $\text{Na}^+$ ,  $\text{K}^+$ ,  $\text{Mg}^{2+}$ ,  $\text{Ca}^{2+}$ ,  $\text{Cl}^-$ ,  $\text{HCO}_3^-$ ,  $\text{HPO}_4^{2-}$  and  $\text{SO}_4^{2-}$  were included. The nominal ion concentrations and preparation of SBF are presented in Ref. [27]. All the samples were immersed separately in 30 mL of SBF with an initial pH value of  $7.4 \pm 0.02$  in a water bath at 37 °C. The immersed samples were placed in fresh SBF without agitation every 7 days in order to keep a stable chemical composition and pH value of the SBF. The pH value of the SBF soaked with all samples was monitored every 24 h during the immersion period. Two types of samples were

used for the immersion test. One set were tensile bars cut from sintered rectangular blocks. These were flat tensile bars with a cross section of 1.6 mm × 2 mm and a gauge length of 8 mm (as specified in Ref. [3]). The other set were square samples with a dimension of 10 mm × 10 mm × 10 mm for ion concentration measurement, and the subsequent cytotoxicity test. For the tensile bars, a wide range of immersion times including 15 days, 30 days, 45 days and 60 days were selected. Three tensile pieces were prepared and immersed in SBF solution for each group of immersion time duration. In the case of the square samples, the samples were mounted in epoxy resin before immersion, so one face was exposed, and this was ground with silicon carbide papers up to 1200 grit. The surface area of the square specimens exposed to SBF solution during immersion test was then 10 × 10 mm<sup>2</sup>. The immersion duration for the mounted squared samples in the SBF solution was 7 days. The SBF solutions containing dissolved Fe and Mn ions from the mounted squared samples were diluted by 20 times after a 7-day immersion. The concentration of Fe and Mn ions in the diluted SBF solutions was measured using inductively coupled plasma mass spectrometry (ICP-MS, Agilent). The degradation rates of the sintered Fe–Mn-based alloys were calculated according to the ASTM G59-97 standard [28]:

$$CR = 3.27 \times 10^{-3} \frac{i_{corr} \cdot EW}{\rho} \quad (1)$$

where  $CR$  is the corrosion rate in mm per year,  $i_{corr}$  is the corrosion current density (mA·cm<sup>-2</sup>),  $EW$  is the equivalent weight according to the percent of the alloying elements,  $\rho$  is the density of the sintered Fe–Mn-based alloys. In this study, the  $i_{corr}$  and  $\rho$  are available in the published paper [3], where the  $i_{corr}$  for the binary and ternary alloys is 45 and 34 mA·cm<sup>-2</sup>, while  $\rho$  for the sintered Fe–28Mn and Fe–28Mn–3Si alloys are 6.6 and 6.4 g·cm<sup>-3</sup>. The  $EW$  of the binary and ternary alloys is 27.85 and 27.79.

#### 2.4. Cytotoxicity Testing

Murine fibroblast cells (L-929, ATCC, Manassas, VA, USA) were employed to assess the cytotoxicity of Fe–28Mn-based alloys, and were cultured at 37 °C in a humidified atmosphere of 5% CO<sub>2</sub>. This testing was performed based on ISO 10993-5: 2009 [29]. The medium for L-929 cells culture was Dulbecco's Modified Eagle Medium (DMEM, Gibco, Grand Island, NY, USA), supplemented with 10% fetal calf serum (FCS). The cell viability was tested by an indirect contact method. After a 72 h incubation period, the cultured cells were diluted to a concentration of 2 × 10<sup>4</sup> cells/mL using DMEM media. Then, 1 mL of the diluted cells was placed into each well of a 24-well plate. 1 mL of fresh DMEM medium was also placed into 3 wells of the 24-well plate, which was used as control in this study. The plate seeded with cells was incubated for 24 h at 37 °C in 5% CO<sub>2</sub> for cell attachment.

A resazurin fluorescence assay was used to determine the cell proliferation during the testing. The samples for cytotoxicity testing were SBF solutions containing metallic ions released from the bulk Fe–Mn-based samples after a 7-day immersion test (SBF containing metallic ions, without dilution were used for the cytotoxicity testing in this study). After 24 h, 1 mL of 500 μM resazurin was placed into each well of the plate to replace the cell medium (DMEM). The plate was incubated for 4 h, and then the supernatant in each well was collected and centrifuged at 2000 rpm for 5 min at room temperature. 100 μL of the centrifuged supernatant was placed in triplicate into a 96-well flat bottomed cell culture plate and the fluorescence value was recorded at 530 nm excitation and 590 nm emission using a Perkin Elmer Enspire 2300 Multilabel Reader. The cells without supernatant in each well were washed using 1 mL of phosphate buffered saline (PBS). Subsequently, 800 μL of fresh DMEM medium and 200 μL of sample solution were added into each well of the plate. For the control group, 1 mL of fresh DMEM medium was added. After this, the 24-well plate was returned to incubator overnight for cell growth. The above procedure was repeated daily in the following 4 days. The entire procedure of the test was repeated three times.

## 2.5. Characterisation

The morphologies of all samples were observed by a scanning electron microscope (SEM, FEI Quanta 200F, FEI, Hillsboro, OR, USA). The chemical compositions of the sintered Fe–Mn-based alloys were measured using an X-ray energy dispersive spectrometer (EDS) attached to an SEM. In order to examine the distribution of Fe, Mn and Si elements in the sintered compacts, EDS line scanning was performed on the cross-section of all the sintered samples. The line scanning started from the surface to the core of the sintered samples, which is perpendicular to the surface plane. More details on the measurement of the distribution using EDS are reported elsewhere [30]. Tensile tests were performed using an Instron 3367 universal testing machine (Instron, Norwood, MA, USA) with a cross-head speed of 0.2 mm/min at room temperature. Before the tensile testing, the dimensions of the cross-section of the immersed tensile bars were re-measured for each immersion time. Three tensile samples were tested for each immersion time duration, and average results were reported.

## 3. Results and Discussion

### 3.1. Chemical Composition of the Sintered Fe–Mn-Based Alloys

Figure 1 shows the compositions obtained from EDS on the cross-section of the sintered Fe–Mn-based alloys. As shown in Figure 1, the Mn content on the surface is extremely low ( $\leq 2$  wt %), and it increases parabolically with the increase of the scan distance from the surface until it stabilizes at approximately 27.5 wt %. This reveals that a Mn depletion region (Mn DR) exists in all the sintered compacts. The Mn DR is caused by the sublimation of Mn due to its high vapor pressure during sintering. The literature data illustrate that the vapor pressure of Mn is  $\sim 98$  Pa [31], which is significantly higher than the vacuum level of  $5 \times 10^{-3}$  Pa. This suggests that Mn could sublimate in the furnace chamber during vacuum sintering. Thus, a Mn depletion region forms on the surface of the sintered alloys. Table 1 summarizes the chemical composition and the elemental distribution of Fe, Mn and Si in the sintered Fe–Mn–Si alloys. Both Figure 1 and Table 1 reveal that the distribution of Fe, Mn and Si is homogeneous and the chemical composition of the sintered alloys is close to their nominal compositions (Fe–28 wt % Mn or Fe–28 wt % Mn–3 wt % Si) if it is detected at the region  $\geq$  Mn DR. In the subsequent microstructural characterization, tensile testing and cytotoxicity testing, the Mn DR layers on the surface were removed from all the sintered samples in order to ensure the chemical composition is consistent with their nominal composition.

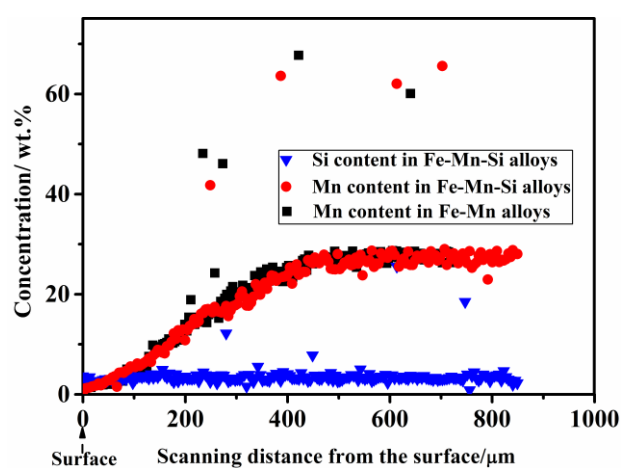


**Figure 1.** The Fe, Mn and Si concentration in Fe–Mn-based alloys as a function of EDS scanning distance from the surface of the cross-section of the sintered alloys at 1200 °C for 3 h.

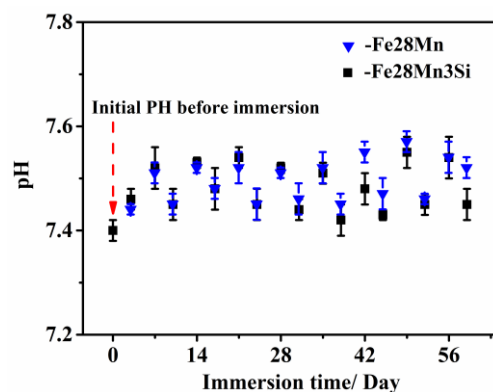
**Table 1.** Thickness of Mn depletion region and average chemical composition of the sintered Fe–Mn-based compacts at 1200 °C for 3 h.

Type of Samples	Thickness of Mn DR <sup>a</sup> (μm)	Chemical Composition (wt %) <sup>b</sup>			
		Mn	Si	O	Fe
Fe–Mn	450 ± 38	27.5 ± 0.6	—	0.3 ± 0.1	Bal.
Fe–Mn–Si	480 ± 35	27.4 ± 0.5	3.1 ± 0.2	0.3 ± 0.1	Bal.

<sup>a</sup> Mn DR is the acronym of Mn depletion region; <sup>b</sup> The chemical compositions of the sintered Fe–Mn-based alloys refer to the chemical compositions outside of the Mn DR regions.

### 3.2. pH Monitoring

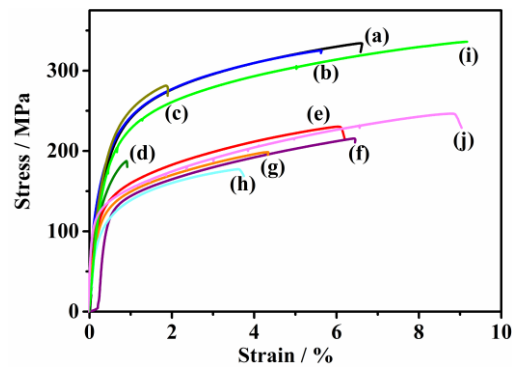
The pH of SBF is an important parameter that should be monitored during immersion testing. This is because a stable pH of SBF close to that of the physiological environment (~7.4) is essential to properly simulate the real degradation behavior of Fe-based DBMs in the human body. In other words, the changes in pH of SBF may have a great impact on the degradation behavior of the implants [32,33]. As for Fe-based DBMs, the corrosion of Fe in SBF solution generates OH<sup>-</sup> [4,9], which may increase the pH value of SBF and exceed the physiological pH range of ~7.4. This creates a non-realistic aqueous environment, which deviates from the situation in the human body. Consequently, the degradation behavior of Fe–Mn-based DBMs in SBF solution may fail to sufficiently reflect what happens in the human body. Figure 2 shows that the pH value of the SBF fluctuates between 7.4 and 7.6 during the immersion period (0–60 days), which is in agreement with the real pH in the human body. This is beneficial to obtain in vitro degradation (corrosion) behavior of the proposed Fe–Mn-based DBMs, which is similar to the situation in the human body. In our case, the proper pH range (7.4–7.6) of SBF during all the immersion period can ensure that the corrosion behavior and ion releasing rates in SBF are consistent with those in the human body. Consequently, the collected data on tensile properties and cytotoxicity in the following sections can be used to predict corrosion behavior in a physiological environment.

**Figure 2.** Comparison of pH over immersion duration for Fe–Mn-based alloys.

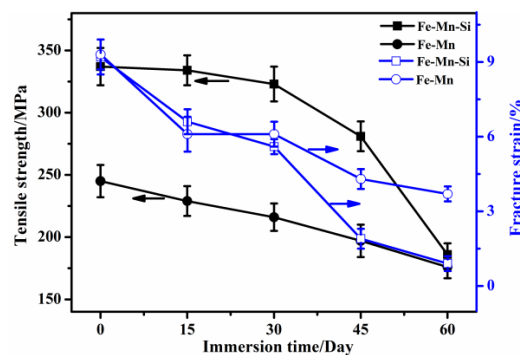
### 3.3. Tensile Properties of the Immersed Fe–Mn-Based Alloys

Figure 3 illustrates the engineering stress-strain curves of the immersed Fe–28Mn-based specimens. All the curves present characteristic strain hardening. The ultimate tensile strength (UTS) and fracture strain ( $\epsilon$ ) of all the immersed samples are summarized in Figure 4. In general, the UTS and  $\epsilon$  of both the ternary and binary specimens decrease with increasing immersion time. It is noted that a significant decrease in UTS of the ternary Fe–Mn–Si specimens occurs when the immersion duration is  $\geq 45$  days. In detail, the UTS of the ternary samples immersed for 30 days is only reduced by ~4.2% compared to their counterparts with no immersion, while those for 45 days and 60 days are decreased by ~16.6% and 45%, respectively. In contrast, immersion time exhibits less influence on the UTS of the binary

Fe–Mn specimens with respect to their ternary Fe–Mn–Si counterparts. For instance, the UTS of the binary Fe–Mn specimens immersed for 60 days decreases by ~28.2% compared to their counterparts with no immersion. This is far less than their ternary Fe–Mn–Si counterparts (~45%) immersed for 60 days. Interestingly, the  $\epsilon$  evolutions of both the binary Fe–Mn and ternary Fe–Mn–Si alloys present a similar trend to that of the UTS. For instance, the  $\epsilon$  of the ternary Fe–Mn–Si specimens immersed for 45 days was 1.93%, only ~1/5 that of the samples with no immersion.



**Figure 3.** Tensile stress-strain curves of the sintered Fe–28Mn-based alloys immersed in SBF solution for various durations: (a) Fe–28Mn–3Si alloys immersed for 15 days; (b) Fe–28Mn–3Si alloys immersed for 30 days; (c) Fe–28Mn–3Si alloys immersed for 45 days; (d) Fe–28Mn–3Si alloys immersed for 60 days; (e) Fe–28Mn alloys immersed for 15 days; (f) Fe–28Mn alloys immersed for 30 days; (g) Fe–28Mn alloys immersed for 45 days; (h) Fe–28Mn alloys immersed for 60 days; (i) Fe–28Mn–3Si alloys with no immersion; (j) Fe–28Mn alloys with no immersion.



**Figure 4.** The evolution of the tensile strength and fracture strain of the sintered Fe–Mn-based alloys as a function of immersion time in SBF solution.

The tensile properties of the immersed Fe–Mn-based samples can be closely related to their microstructure and fracture behavior. Figure 5 shows the surface morphologies of the sintered Fe–Mn-based samples with different immersion durations. There exist some prolate pores (Arrow P in Figure 5) and many inclusions (Arrow Q in Figure 5) visible in the sintered Fe–Mn-based alloys with no immersion. The pores are isolated and smooth, which is a typical microstructure at their final sintering stage. The EDS results demonstrate that the inclusions are oxide-rich in Mn. More details on the microstructure and inclusions of the sintered Fe–Mn-based alloys can be seen in Ref. [30]. It appears that the regions around the pores are susceptible to corrosion. This is evidenced that the pore size (Arrow T and shaded area S in Figure 5) and the total pore areas in all the samples increase with increasing the immersion time. It is interesting to note that the majority of the pores after immersion are irregular and sharp-edged. Such pore structures are stress concentrators and therefore decrease the tensile properties, both fracture strength and fracture strain [34–36]. Thus,

the tensile properties, especially the fracture strain of the sintered Fe–Mn-based alloys, significantly degrade with the increase of immersion time due to the increased number of irregular and sharp-edged pores. In addition, the reduction on the cross-sectional areas of the immersed bars could be another important factor to the decrease in their tensile properties. This could be supported by combined results on degradation rates and EDS data. The corrosion (degradation) rates of the sintered binary and ternary alloys calculated based on Equation (1) are  $\sim 0.56$  and  $0.48$  mm per year. For another, the EDS results (Table 2) on the surface of the immersed Fe–Mn-based alloys demonstrate that the oxygen content on the surface increases with the increase of immersion time. This reflects that more corrosion products (oxides) formed with the increase of the immersion time. In this case, the effective load-bearing cross-sectional areas are likely to decrease with increasing immersion time. Particularly, the oxygen content on the surface of the samples immersed for  $\geq 45$  days is remarkably higher than their counterparts for  $\leq 15$  days, indicating that a more severe reduction on the cross-sectional areas is likely to happen in the immersed alloys soaking for  $\geq 45$  days. Thus, both results reveal that the reduction on the cross-sectional area of the tensile bars may occur during immersion. Nevertheless, the cross-section of the tensile samples were re-measured, thereby the reduced tensile properties are mainly a consequence of corrosion and the microstructural change after immersion.

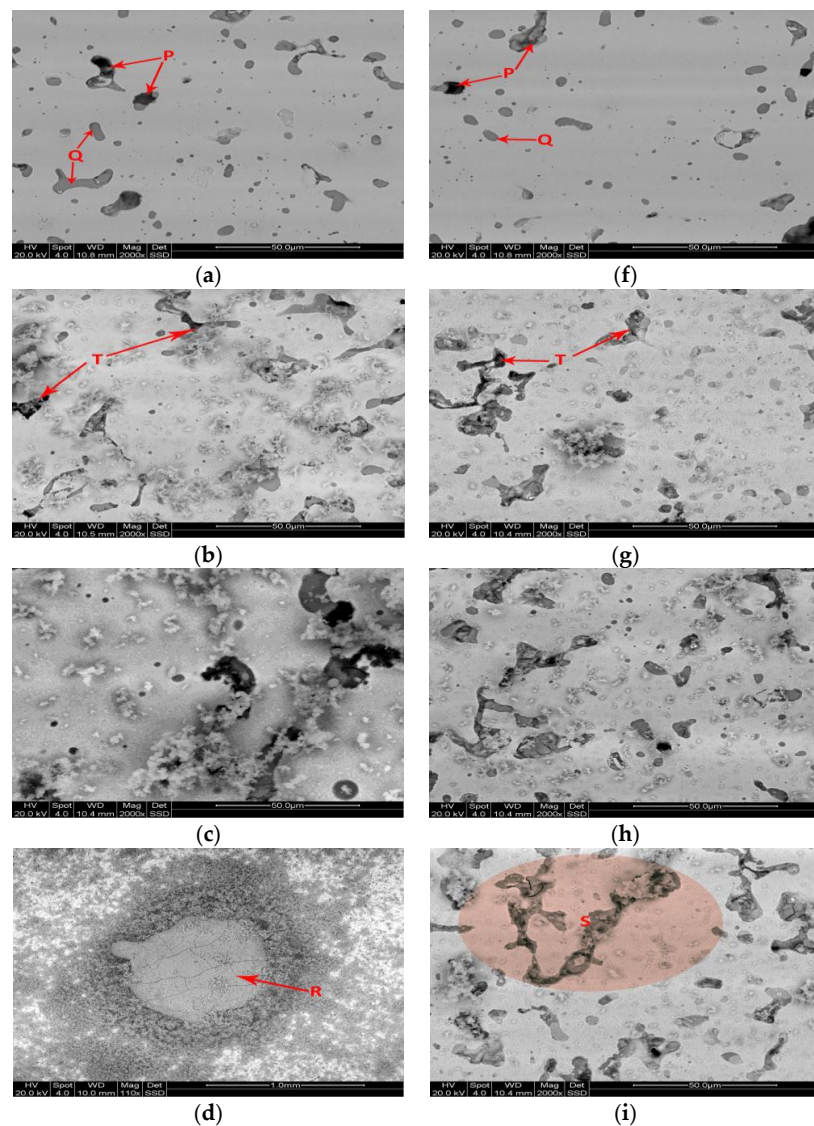
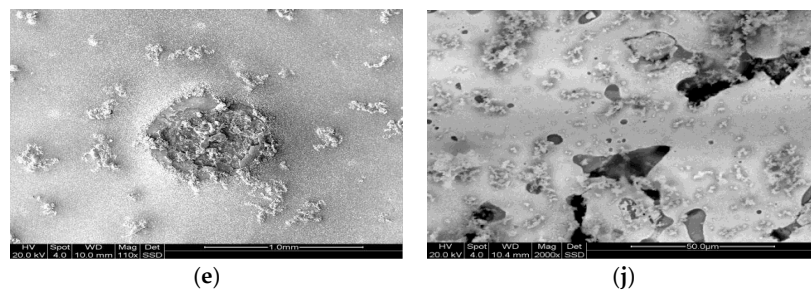


Figure 5. Cont.



**Figure 5.** SEM micrographs of the sintered Fe–28Mn-based alloys immersed in SBF solution for different durations: (a) Fe–28Mn–3Si alloy with no immersion; (b) Fe–28Mn–3Si alloys immersed for 15 days; (c) Fe–28Mn–3Si alloys immersed for 30 days; (d) Fe–28Mn–3Si alloys immersed for 45 days; (e) Fe–28Mn–3Si alloys immersed for 60 days; (f) Fe–28Mn alloy with no immersion; (g) Fe–28Mn alloys immersed for 15 days; (h) Fe–28Mn alloys immersed for 30 days; (i) Fe–28Mn alloys immersed for 45 days; (j) Fe–28Mn alloys immersed for 60 days. (Note: Arrow P, Q, T, R and shaded area S are the focus of interest in the sintered alloys with different immersion durations).

**Table 2.** Average EDS results on the surface of the immersed Fe–Mn-based samples with different immersion times.

Type of Samples	Immersion Time (Day)	Chemical Composition (wt %)						
		O	P	Ca	C	Mn	Si	Fe
Fe–Mn	15	5.3 ± 0.1	2.5 ± 0.1	0.8 ± 0.1	2.6 ± 0.1	23.9 ± 0.5	-	Bal.
	30	9.6 ± 0.2	2.8 ± 0.2	1.2 ± 0.2	3 ± 0.4	23.5 ± 0.7	-	Bal.
	45	15.8 ± 0.3	5.1 ± 0.2	2.1 ± 0.2	3.5 ± 0.3	22.8 ± 0.6	-	Bal.
	60	18.5 ± 0.7	4.5 ± 0.6	2.1 ± 0.3	3.3 ± 0.6	23.2 ± 0.8	-	Bal.
Fe–Mn–Si	15	5.1 ± 0.2	2.9 ± 0.1	1.5 ± 0.1	3.5 ± 0.2	24 ± 0.5	2.3 ± 0.2	Bal.
	30	10.8 ± 0.5	3.3 ± 0.4	1.4 ± 0.3	2.8 ± 0.3	23.1 ± 0.6	2 ± 0.4	Bal.
	45	23.7 ± 0.4	9.9 ± 0.3	3 ± 0.2	4 ± 0.4	17.5 ± 0.2	1.2 ± 0.2	Bal.
	60	25.9 ± 0.9	9.5 ± 0.5	2.7 ± 0.2	3.5 ± 0.2	18 ± 0.4	1.5 ± 0.5	Bal.

It is noted that localized macroscopic pits (Arrow R in Figure 5) form in the ternary Fe–Mn–Si samples. Similar pits were also found in the casting Fe–Mn–Si alloys immersed in SBF for 180 days by Liu et al. [37]. However, the formation mechanism of the large pits is still unclear. The formation of the macroscopic pits may be an essential factor to the sharp decrease of the fracture strain occurring in the ternary Fe–Mn–Si alloys when the immersed time increases to  $\geq 45$  days. The localized macroscopic pits could be sites for crack initiation due to stress concentration [38,39], and therefore lead to the deterioration in the fracture strain of the sintered Fe–Mn–Si alloys. Also, Figure 4 reveal that the fracture strain of the binary Fe–Mn samples immersed for  $\geq 45$  days is higher than their ternary Fe–Mn–Si counterparts, this may benefit from the absence of macroscopic pits in the immersed binary Fe–Mn samples.

The weak mechanical properties of both the binary Fe–Mn and ternary Fe–Mn–Si samples after long immersion time ( $\geq 45$  days) can be also reflected in their fractography. Figure 6c,g shows that the number of dimples in both samples immersed for 45 days decreases remarkably with respect to their counterparts with no immersion. This firmly proves inferior mechanical properties of both the binary and ternary samples immersed for a long time ( $\geq 45$  days).

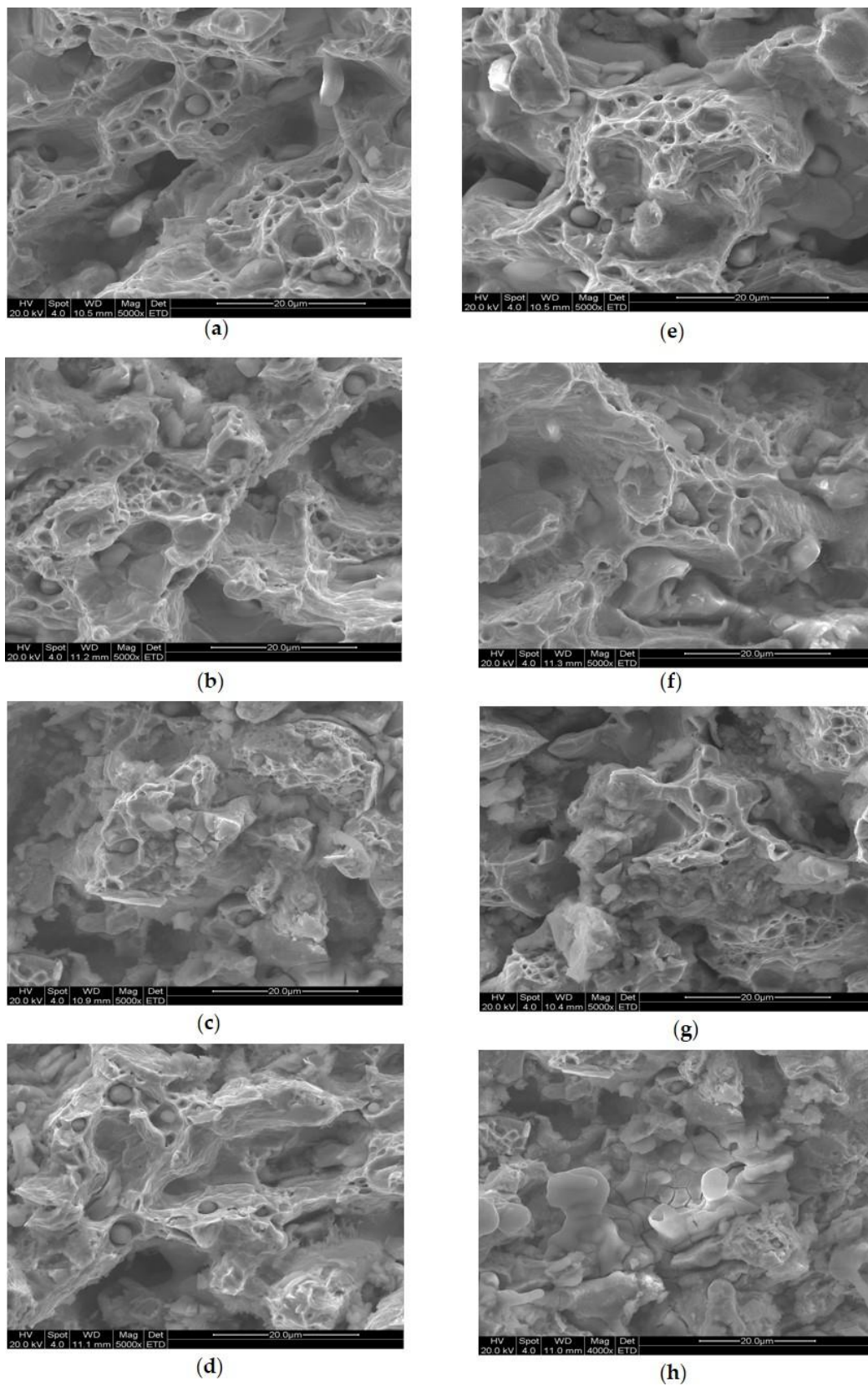


**Figure 6.** Fracture surface of the as-sintered Fe-28Mn-based alloys immersed in SBF solution for different durations: (a) Fe-28Mn-3Si alloy with no immersion; (b) Fe-28Mn-3Si alloys immersed for 15 days; (c) Fe-28Mn-3Si alloys immersed for 45 days; (d) Fe-28Mn-3Si alloys immersed for 60 days; (e) Fe-28Mn alloys without immersion; (f) Fe-28Mn alloys immersed for 15 days; (g) Fe-28Mn alloys immersed for 45 days; (h) Fe-28Mn alloys immersed for 60 days.

### 3.4. Biocompatibility of the Sintered Fe–Mn-Based Alloys

The combined mechanical properties and biocompatibility of the fabricated Fe–Mn-based temporary implants determine whether they are adequate to be implanted safely in the human body [40]. In general, the mechanical properties degrade along with the increase of implantation time due to the aggressive environment in the human body. The failure of the structural integrity before the recovery of the diseased tissues can impede the healing of the diseased tissues or even cause them to deteriorate [1]. Thus, the tensile properties of the sintered Fe–Mn-based alloys were measured as a function of immersion time in SBF solution as a preliminary prediction of the life span of the sintered Fe–Mn–Si alloys in the human body. However, fabricated materials with good mechanical properties are impossible to use as biomaterials if they lack enough biocompatibility with the human body. One key issue relating to the biocompatibility is the cytotoxicity of the implanted devices [4,41]: The metal ions release in the human body when they are under a corrosive physiological environment. However, excessive metal ions may be toxic to the human body and therefore be harmful to the patient. Thus, *in vitro* cytotoxicity testing is an essential step to determine whether it is necessary to proceed further in *in vivo* biocompatibility testing.

Figure 7 presents the Fe and Mn ion concentration in the SBF solutions after the bulk samples were soaked for 7 days. It is noted that no Si ions are detected in SBF solution where the bulk Fe–Mn–Si samples were immersed. This reveals that the releasing rate of Si ions in SBF solution is very slow and can be neglected. The Fe and Mn ion concentrations released into the SBF from the ternary Fe–Mn–Si samples are ~0.392 and 0.13 ppm, respectively. Liu et al. [37] also investigated the ion concentration released in the immersed SBF. Liu's research reveals that both the Fe and Mn ion releasing rates in SBF are less than 10 ppm after 10-day immersion. This is lower than the results in this study. The improvement of the ion releasing concentration can be attributed to the porosities caused by powder sintering route. Previous studies demonstrated that the overall porosities of the PM Fe–Mn-based alloys in this study are ~15% (in volume percent) [3,30]. The porosities in the PM alloys can provide more surface area for degradation. Thus, the ion releasing rate of the PM Fe–Mn-based alloys in this study is higher than the casting alloys.

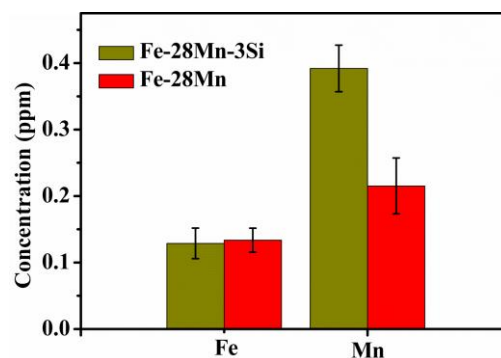


**Figure 7.** Concentration of Fe and Mn ions releasing from the sintered Fe–28Mn-based alloys in SBF solution after a 7-day immersion test.

Interestingly, the Fe ion concentration released from the binary Fe–Mn samples is almost equal to that from the ternary Fe–Mn–Si samples. However, Mn ion concentration released from the binary alloy is only around 55% of the ternary alloys. This shows that the overall ion release rate of the ternary Fe–Mn–Si samples in SBF is much faster than their binary Fe–Mn counterparts. Our previous research [3] reveals that the sintered Fe–Mn–Si alloy consists of a dual  $\gamma$ -austenite and  $\epsilon$ -martensite, while the binary Fe–Mn alloy only comprises a single  $\gamma$ -austenite. Relevant research suggests [28,37,42] that the higher ion releasing concentration in the ternary PM Fe–Mn–Si alloy may benefit from the galvanic corrosion between  $\gamma$ -austenite and  $\epsilon$ -martensite.

Figure 8 shows the results of the in vitro cytotoxicity test. It can be seen that fluorescence values of both the ternary Fe–Mn–Si and binary Fe–Mn samples increases with the increase of culture time. In other words, the ions released from the corroding binary and ternary bulk samples did not inhibit the proliferation of L929 cells. This confirms that the sintered Fe–Mn-based alloys present good cell viability in L929 cells.

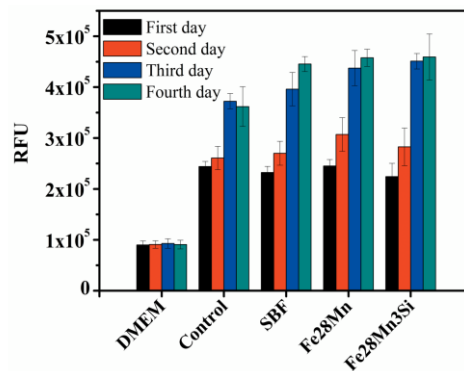


**Figure 8.** Proliferation of L929 cells in presence of SBF solution containing Fe and Mn ions (Note: Relative fluorescence units are abbreviated as RFU).

#### 4. Conclusions

In this study, the relationship between the immersion duration and tensile properties of the immersed Fe–Mn-based alloys in SBF solution were investigated. In addition, the biocompatibility of the sintered Fe–Mn-based alloys was assessed. In general, the tensile properties of the immersed samples decreased with the increase of immersion time. A severe decrease of fracture strain occurred in both the binary Fe–Mn and ternary Fe–Mn–Si samples after being immersed for  $\geq 45$  days. For example, the fracture strain of the ternary Fe–Mn–Si and binary Fe–Mn alloys immersed for 45 days decreased by  $\sim 80\%$  and  $55\%$ , respectively, as compared to those with no immersion. The binary Fe–Mn alloys presented better tensile properties than their ternary Fe–Mn–Si counterparts, if under the same immersion duration. The concentration of total ions in SBF released from the ternary Fe–Mn–Si samples was doubled, as compared to their binary Fe–Mn counterparts. The short-term cell viability test demonstrates that both the ternary Fe–Mn–Si and binary Fe–Mn alloys presented no inhibition on the proliferation of Murine fibroblast cells (L929 cells) at the first 7-day immersion duration.

**Acknowledgments:** Zhigang Xu acknowledges China Scholarship Council (CSC) for providing a doctoral scholarship. The authors would like to thank Simon Swift and Benedict Uy (Faculty of Medical and Health Sciences at The University of Auckland, New Zealand) for their assistance on biocompatibility testing.

**Author Contributions:** All authors are involved in designing the experiments. Zhigang Xu performed the sample preparation, data analysis and manuscript writing and editing. Michael Hodgson and Peng Cao contributed to manuscript proofreading.

**Conflicts of Interest:** The authors declare no conflicts of interest.

#### References

1. Hermawan, H.; Dubé, D.; Mantovani, D. Developments in metallic biodegradable stents. *Acta Biomater.* **2010**, *6*, 1693–1697. [[CrossRef](#)] [[PubMed](#)]
2. Moravej, M.; Purnama, A.; Fiset, M.; Couet, J.; Mantovani, D. Electroformed pure iron as a new biomaterial for degradable stents: In vitro degradation and preliminary cell viability studies. *Acta Biomater.* **2010**, *6*, 1843–1851. [[CrossRef](#)] [[PubMed](#)]
3. Xu, Z.; Hodgson, M.A.; Cao, P. A comparative study of powder metallurgical (PM) and wrought Fe–Mn–Si alloys. *Mater. Sci. Eng. A* **2015**, *630*, 116–124. [[CrossRef](#)]

4. Schinhammer, M.; Gerber, I.; Hänzi, A.C.; Uggowitzer, P.J. On the cytocompatibility of biodegradable Fe-based alloys. *Mater. Sci. Eng. C* **2013**, *33*, 782–789. [[CrossRef](#)] [[PubMed](#)]
5. Francis, A.; Yang, Y.; Virtanen, S.; Boccaccini, A. Iron and iron-based alloys for temporary cardiovascular applications. *J. Mater. Sci. Mater. Med.* **2015**, *26*, 1–16. [[CrossRef](#)] [[PubMed](#)]
6. Xu, Z.; Hodgson, M.A.; Cao, P. Microstructure and degradation behavior of forged Fe–Mn–Si alloys. *Int. J. Mod. Phys. B* **2015**, *29*, 1–6. [[CrossRef](#)]
7. Song, G.; Song, S. A possible biodegradable magnesium implant material. *Adv. Eng. Mater.* **2007**, *9*, 298–302. [[CrossRef](#)]
8. Mintz, G.S.; Hoffmann, R.; Mehran, R.; Pichard, A.D.; Kent, K.M.; Satler, L.F.; Popma, J.J.; Leon, M.B. In-stent restenosis: The Washington Hospital Center experience. *Amer. J. Cardiol.* **1998**, *81*, 7E–13E. [[CrossRef](#)]
9. Hermawan, H.; Purnama, A.; Dube, D.; Couet, J.; Mantovani, D. Fe–Mn alloys for metallic biodegradable stents: Degradation and cell viability studies. *Acta Biomater.* **2010**, *6*, 1852–1860. [[CrossRef](#)] [[PubMed](#)]
10. Hermawan, H.; Moravej, M.; Dubé, D.; Fiset, M.; Mantovani, D. Degradation behaviour of metallic biomaterials for degradable stents. *Adv. Mater. Res.* **2007**, *15*, 113–118. [[CrossRef](#)]
11. Tang, Y.C.; Katsuma, S.; Fujimoto, S.; Hiromoto, S. Electrochemical study of Type 304 and 316L stainless steels in simulated body fluids and cell cultures. *Acta Biomater.* **2006**, *2*, 709–715. [[CrossRef](#)] [[PubMed](#)]
12. Oak, J.J.; Inoue, A. Attempt to develop Ti-based amorphous alloys for biomaterials. *Mater. Sci. Eng. A* **2007**, *449*, 220–224. [[CrossRef](#)]
13. Takaichi, A.; Nakamoto, T.; Joko, N.; Nomura, N.; Tsutsumi, Y.; Migita, S.; Doi, H.; Kurosu, S.; Chiba, A.; Wakabayashi, N. Microstructures and mechanical properties of Co–29Cr–6Mo alloy fabricated by selective laser melting process for dental applications. *J. Mech. Behav. Biomed.* **2013**, *21*, 67–76. [[CrossRef](#)] [[PubMed](#)]
14. Nasab, M.B.; Hassan, M.R. Metallic biomaterials of knee and hip-A review. *Trends Biomater. Artif. Organs* **2010**, *24*, 69–82.
15. Milošev, I.; Pišot, V.; Campbell, P. Serum levels of cobalt and chromium in patients with Sikomet metal–metal total hip replacements. *J. Orthop. Res.* **2005**, *23*, 526–535. [[CrossRef](#)] [[PubMed](#)]
16. Wegener, B.; Sievers, B.; Utzschneider, S.; Müller, P.; Jansson, V.; Rößler, S.; Nies, B.; Stephani, G.; Kieback, B.; Quadbeck, P. Microstructure, cytotoxicity and corrosion of powder-metallurgical iron alloys for biodegradable bone replacement materials. *Mater. Sci. Eng. B* **2011**, *176*, 1789–1796. [[CrossRef](#)]
17. Witte, F. The history of biodegradable magnesium implants: A review. *Acta Biomater.* **2010**, *6*, 1680–1692. [[CrossRef](#)] [[PubMed](#)]
18. Moravej, M.; Mantovani, D. Biodegradable metals for cardiovascular stent application: Interests and new opportunities. *Int. J. Mol. Sci.* **2011**, *12*, 4250–4270. [[CrossRef](#)] [[PubMed](#)]
19. Andani, M.T.; Moghaddam, N.S.; Haberland, C.; Dean, D.; Miller, M.J.; Elahinia, M. Metals for bone implants. Part 1. Powder metallurgy and implant rendering. *Acta Biomater.* **2014**, *10*, 4058–4070. [[CrossRef](#)] [[PubMed](#)]
20. Hanks, C.T.; Wataha, J.C.; Sun, Z. In vitro models of biocompatibility: A review. *Dent. Mater.* **1996**, *12*, 186–193. [[CrossRef](#)]
21. Říhová, B. Biocompatibility of biomaterials: Hemocompatibility, immunocompatibility and biocompatibility of solid polymeric materials and soluble targetable polymeric carriers. *Adv. Drug Del. Rev.* **1996**, *21*, 157–176. [[CrossRef](#)]
22. Kraus, T.; Moszner, F.; Fischerauer, S.; Fiedler, M.; Martinelli, E.; Eichler, J.; Witte, F.; Willbold, E.; Schinhammer, M.; Meischel, M. Biodegradable Fe-based alloys for use in osteosynthesis: Outcome of an in vivo study after 52 weeks. *Acta Biomater.* **2014**, *10*, 3346–3353. [[CrossRef](#)] [[PubMed](#)]
23. Drynda, A.; Hassel, T.; Bach, F.W.; Peuster, M. In vitro and in vivo corrosion properties of new iron–manganese alloys designed for cardiovascular applications. *J. Biomed. Mater. Res. B* **2015**, *103*, 649–660. [[CrossRef](#)] [[PubMed](#)]
24. Oriňaková, R.; Oriňak, A.; Giretová, M.; Medvecký, L.U.; Kupková, M.; Hrubovčáková, M.; Maskal'ová, I.; Macko, J.; Kal'avský, F. A study of cytocompatibility and degradation of iron-based biodegradable materials. *J. Biomater. Appl.* **2016**, *30*, 1060–1070. [[CrossRef](#)] [[PubMed](#)]
25. Ratner, B.; Northrup, S.; Anderson, J. Biological testing of biomaterials. In *Biomaterials Science: An Introduction to Materials in Medicine*, 2nd ed.; Elsevier: San Diego, CA, USA, 2004; pp. 355–360.
26. Morais, J.M.; Papadimitrakopoulos, F.; Burgess, D.J. Biomaterials/tissue interactions: Possible solutions to overcome foreign body response. *AAPS J.* **2010**, *12*, 188–196. [[CrossRef](#)] [[PubMed](#)]

27. Kokubo, T.; Takadama, H. How useful is SBF in predicting in vivo bone bioactivity? *Biomaterials* **2006**, *27*, 2907–2915. [[CrossRef](#)] [[PubMed](#)]
28. Hermawan, H.; Dubé, D.; Mantovani, D. Degradable metallic biomaterials: Design and development of Fe–Mn alloys for stents. *J. Biomed. Mater. Res. A* **2010**, *93*, 1–11. [[CrossRef](#)] [[PubMed](#)]
29. International Standardization Organization. International Standardization Organization. ISO 10993-5: Biological evaluation of medical devices. In *Part 5: Tests for in Vitro Cytotoxicity*; ISO: Geneva, Switzerland, 2009.
30. Xu, Z.; Hodgson, M.A.; Cao, P. Effects of Mechanical Milling and Sintering Temperature on the Densification, Microstructure and Tensile Properties of the Fe–Mn–Si Powder Compacts. *J. Mater. Sci. Technol.* **2016**, *32*, 1161–1170. [[CrossRef](#)]
31. Šalák, A.; Selecká, M.; Bureš, R. Manganese in ferrous powder metallurgy. *Powder Metall. Prog.* **2001**, *1*, 41–58.
32. Kirkland, N.; Birbilis, N.; Staiger, M. Assessing the corrosion of biodegradable magnesium implants: A critical review of current methodologies and their limitations. *Acta Biomater.* **2012**, *8*, 925–936. [[CrossRef](#)] [[PubMed](#)]
33. Schinhammer, M.; Hofstetter, J.; Wegmann, C.; Moszner, F.; Löffler, J.F.; Uggowitzer, P.J. On the immersion testing of degradable implant materials in simulated body fluid: Active pH regulation using CO<sub>2</sub>. *Adv. Eng. Mater.* **2013**, *15*, 434–441. [[CrossRef](#)]
34. Holmes, J.; Queeney, R. Fatigue crack initiation in a porous steel. *Powder Metall.* **1985**, *28*, 231–235. [[CrossRef](#)]
35. Zhu, S.; Yang, X.; Fu, D.; Zhang, L.; Li, C.; Cui, Z. Stress-strain behavior of porous NiTi alloys prepared by powders sintering. *Mater. Sci. Eng. A* **2005**, *408*, 264–268. [[CrossRef](#)]
36. Kubicki, B. Stress Concentration at Pores in Sintered Materials. *Powder Metall.* **1995**, *38*, 295–298. [[CrossRef](#)]
37. Liu, B.; Zheng, Y.; Ruan, L. In vitro investigation of Fe<sub>30</sub>Mn<sub>6</sub>Si shape memory alloy as potential biodegradable metallic material. *Mater. Lett.* **2011**, *65*, 540–543. [[CrossRef](#)]
38. Cerit, M.; Genel, K.; Eksi, S. Numerical investigation on stress concentration of corrosion pit. *Eng. Fail. Anal.* **2009**, *16*, 2467–2472. [[CrossRef](#)]
39. Anderson, T.L.; Anderson, T. *Fracture Mechanics: Fundamentals and Applications*; CRC Press: Boca Raton, FL, USA, 2005.
40. Gong, S.; Wang, H.; Sun, Q.; Xue, S.-T.; Wang, J.-Y. Mechanical properties and in vitro biocompatibility of porous zein scaffolds. *Biomaterials* **2006**, *27*, 3793–3799. [[CrossRef](#)] [[PubMed](#)]
41. Čapek, J.; Kubásek, J.; Vojtěch, D.; Jablonská, E.; Lipov, J.; Ruml, T. Microstructural, mechanical, corrosion and cytotoxicity characterization of the hot forged FeMn30 (wt %) alloy. *Mater. Sci. Eng. C* **2016**, *58*, 900–908. [[CrossRef](#)] [[PubMed](#)]
42. Cheng, J.; Zheng, Y. In vitro study on newly designed biodegradable Fe-X composites (X = W, CNT) prepared by spark plasma sintering. *J. Biomed. Mater. Res. B* **2013**, *101*, 485–497. [[CrossRef](#)] [[PubMed](#)]



© 2016 by the authors; licensee MDPI, Basel, Switzerland. This article is an open access article distributed under the terms and conditions of the Creative Commons Attribution (CC-BY) license (<http://creativecommons.org/licenses/by/4.0/>).